frontiers in Earth Science

ORIGINAL RESEARCH
published: 29 September 2021
doi: 10.3389/feart.2021.739507

Simulation of Rapid Intensification of Super Typhoon Lekima (2019). Part I: Evolution Characteristics of Asymmetric Convection Under Upper-Level Vertical Wind Shear

Qijun Huang[1], *Xuyang Ge*[1]* *and Melinda Peng*[2]

[1]*Key Laboratory of Meteorological Disaster of Ministry of Education, Joint International Research Laboratory of Climate and Environment Change, Collaborative Innovation Center on Forecast and Evaluation of Meteorological Disasters, Nanjing University of Information Science and Technology, Nanjing, China,* [2]*University of Colorado, Denver, CO, United States*

The role of the upper-level vertical wind shear (VWS) on the rapid intensification (RI) of super typhoon Lekima (2019) is investigated with a high-resolution numerical simulation. Our simulation shows that under moderate upper-level easterly VWS, the tilting-induced convective asymmetry is transported from the initially downshear quadrant to the upshear quadrant and wrapped around the storm center by the cyclonic flow of the storm while moving inward. This process enhances upward motions at the upshear flank and creates upper-level divergent flow. As such, the establishment of outflow acts against the environmental flow to reduce the VWS, allowing vertical alignment of the storm. The organized outflow plays an important role in sustaining the inner-core deep convection by modulating the environmental upper-level thermal structure. Accompanying deep convective bursts (CBs), cold anomalies are generated in the tropopause layer due to the adiabatic cooling by the upward motion and radiative process associated with the cloud anvil. Physically, cold anomalies at the tropopause locally destabilize the atmosphere and enhance the convections and the secondary circulation. The CBs continue to develop episodically through this process as they wrap around the storm center to form a symmetric eyewall. The results suggest that deep convections are capable of reducing the upper-level VWS, promoting the development of upper-level outflow. Lekima overcame the less favorable environment and eventually intensified to become a super typhoon.

Keywords: tropical cyclone, rapid intensification, upper vertical shear, outflow pattern, asymmetric convection

OPEN ACCESS

Edited by:
Guanghua Chen,
Institute of Atmospheric Physics, Chinese Academy of Sciences, China

Reviewed by:
Donglei Shi,
Institute of Atmospheric Physics (CAS), China
Eric Hendricks,
National Center for Atmospheric Research (UCAR), United States

***Correspondence:**
Xuyang Ge
xuyang@nuist.edu.cn

Specialty section:
This article was submitted to Atmospheric Science, a section of the journal Frontiers in Earth Science

Received: *11 July 2021*
Accepted: *17 August 2021*
Published: *29 September 2021*

Citation:
Huang Q, Ge X and Peng M (2021) Simulation of Rapid Intensification of Super Typhoon Lekima (2019). Part I: Evolution Characteristics of Asymmetric Convection Under Upper-Level Vertical Wind Shear. Front. Earth Sci. 9:739507. doi: 10.3389/feart.2021.739507

INTRODUCTION

Although the track forecasts of tropical cyclones (TCs) have been improved progressively, intensity prediction remains as a big challenge for the TC community (DeMaria et al., 2014), particularly during the rapid intensification (RI) with winds increased by at least 30 knots in a 24-hour period. The operational prediction of RI is particularly difficult (Titley and Elsberry, 2000; Elsberry et al., 2007). It has been well realized that the RI is ascribed to the multi-scale interactions, involving environmental, oceanic, and inner-core processes (Kaplan and DeMaria, 2003; Emanuel et al., 2004;

Kaplan et al., 2015). Statistical studies reveal that there are significant differences in both oceanic conditions (Wang and Wu, 2004; Zeng et al., 2010; Zhang et al., 2017) and atmospheric conditions for developing versus non-developing TCs (Ge et al., 2013; Zhang and Tao, 2013; Gu et al., 2015). Among them, the environmental vertical wind shear (VWS) has long been considered as one of the key factors controlling the intensity of TCs (Emanuel et al., 2004; Zeng et al., 2007; Zeng et al., 2008; Wang et al., 2015; Chen et al., 2017). Several negative effects of VWS on the intensification have been proposed, including: 1) upper-level dilution of the TC warm core (Frank and Ritchie, 2001); 2) dry intrusion of mid-level air into the TC eyewall (Tang and Emanuel, 2010; Ge et al., 2013; Kanada and Wada, 2015); and 3) the so-called mid-level "ventilation" effect (Riemer et al., 2010; Tang and Emanuel, 2010; Tang and Emanuel, 2012; Riemer and Laliberté, 2015). In short, these studies suggest that due to the evaporation of precipitation or ambient intrusion from outside the storm's inner region, the air with low equivalent potential temperature (θ_e) reduces eyewall moist entropy located downshear-left and suppresses convection within the eyewall.

In general, the VWS acts to tilt the TC vortex, creating pronounced asymmetries in TC structure and rainfall pattern and thus is not favorable for TC development. Statistically, there exists a wavenumber one convective asymmetry with strong updrafts in the downshear-left flank during the intensifying period under the vertical wind shear (Rogers 2016). The linkage between convective updrafts around the storm center and the RI process has been widely examined. From both observation and numerical simulations, TCs experiencing RI episodes usually have a relatively large amount of deep and vigorous convective bursts (CBs) inside the radius of maximum wind (RMW) (Braun, 2013; Chen and Zhang, 2013; Rogers et al., 2013; Sanger et al., 2014; Chen and Gopalakrishnan, 2015; Rogers et al., 2015; Smith and Montgomery, 2015; Rogers et al., 2016). The axisymmetrization process associated with these rotating convective updrafts in and around the developing eyewall region also contributes to TC intensification. For instance, Bhalachandran et al. (2020) found that certain aspects of eddy energetics can potentially serve as early-warning indicators of TC rapid intensity changes. However, different types of downdrafts have different impacts on the TC intensity (Wadler et al., 2018).

The complex interactions between VWS with different structures and convective patterns likely will result in different outcomes for TC intensification. Finocchio et al. (2016) found that the development of a TC is highly sensitive to the shear height and depth. The shear height appears to affect the response of a TC to the tilt by modifying its thermodynamics, while the shear depth controls the height of TC in responding to the tilt. Generally, the shallower and lower the VWS, the more destructive it is to TC's intensification. TC vortices tilt the most under lower-level VWS and are unable to process upshear and realign, thus fail to intensify. Some recent observational and numerical studies (Leighton et al., 2018; Ryglicki et al., 2018a; Ryglicki et al., 2018b; Li et al., 2020) found that TCs can experience an RI under moderate VWS (e.g., 5–10 m s^{-1}). For this atypical class of TCs underwent RI, it is hypothesized that they are closely associated with the tilt-modulated convective asymmetries (TCA). The TCAs, characterized as collections of updrafts, move towards upshear flank to enhance upper-level outflow. The enhanced outflow converges with the environmental winds, creating a dynamic high pressure to decelerate the environmental winds and thus reduced the VWS. Corbosiero and Molinari (2002) suggested that the deep divergent circulations in the active TC can reduce the VWS and act to minimize the tilt of the TC.

Under various VWSs, TC intensity is largely determined by the vertical alignment of TC circulations (Zhang and Tao, 2013) with some conceptual models for the interpretations (Wong and Chan, 2004; Zhang and Kieu, 2006). However, how the VWS precisely influences the convection pattern, and thus the vertical alignment remains unclear. For example, Molinari et al. (2006) pointed out that TC intensification can be promoted under a sheared environment when a TC undergoes a "downshear reformation" to suppress the ventilation effect. This differs from the "upshear realignment" process discussed above. We attempt to explore this scientific question by investigating super typhoon (STY) Lekima (2019) through numerical simulation. As will be shown later, Lekima underwent an RI under moderate upper-level VWS. Some recent studies (Dai et al., 2021; Shi and Chen, 2021) have focused on the different aspects of these particular TC structures (i.e., warm core and asymmetric rainbands). Dai et al. (2021) investigated the quasi-periodic intensification of convective asymmetries in the outer eyewall during the mature stage. In this study, we focus on an early stage (during the period of RI), and the main focus is on the possible interaction between upper outflow and TCA.

The article is organized as follows. In *Model Configurations* section, the numerical model used for the simulation and its configuration are described. The simulated results are presented in *Environment of Lekima* section. The physical understanding is given in *Simulated Results* section. Finally, discussion and summary are given in the last section.

MODEL CONFIGURATIONS

In this study, the Advanced Research Weather Research and Forecasting model (WRF-ARW; version 3.9.1; Davis et al., 2008) is used. Four-nested domains with the horizontal grid spacings of 27, 9, 3, and 1 km, respectively, are configured with two-way interactions between each domain. The outermost domain covers a region of (90°E–155°E, 0°–40°N) (not shown). The vortex-following technique is used to allow the TC-vortex to be always located near the center for the second and the innermost moving-nested domain. There are 45 uneven σ levels in the vertical using terrain-following extending from the surface to the model top at 10 hPa. The model physics includes a Lin microphysics scheme (Lin et al., 1983), including six classes of hydrometeors about water vapor, cloud water, rain, cloud ice, snow, and graupel. Kain–Fritsch convective scheme (Kain and Fritsch, 1993) is applied for the outermost domain only, and YSU turbulent mixing scheme for boundary layer parameterization. For the radiation process, Dudhia

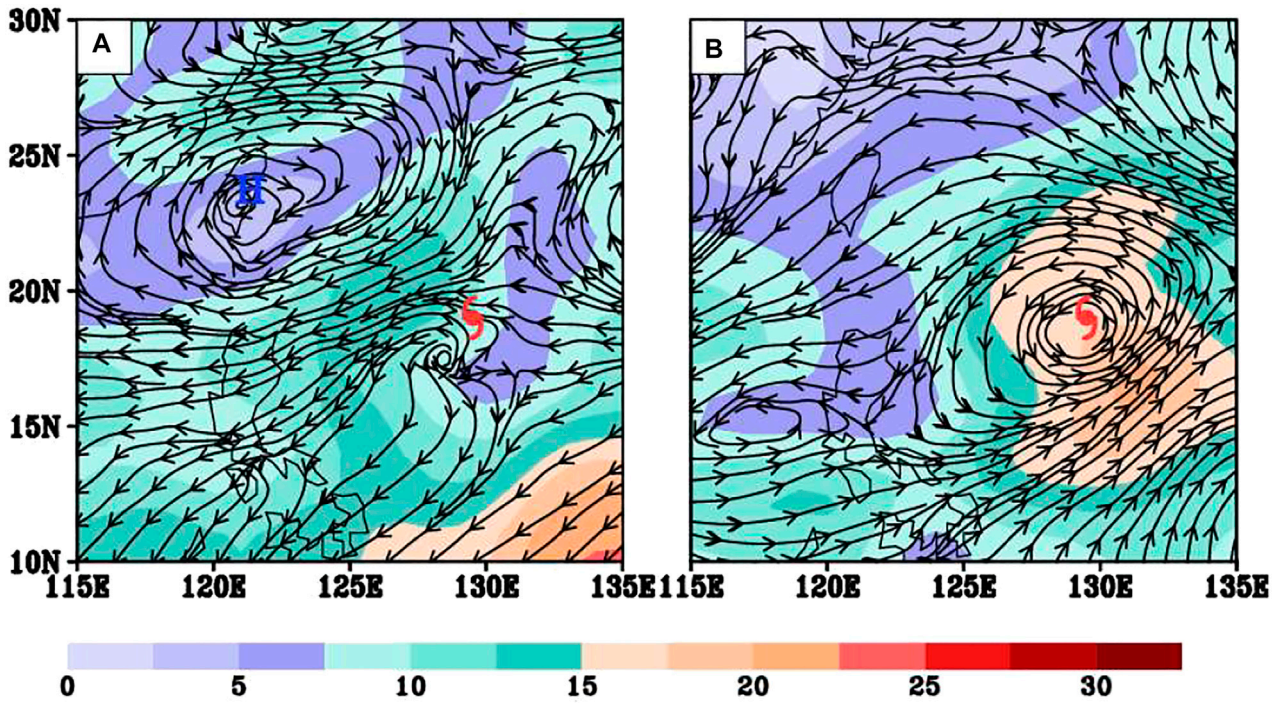

FIGURE 1 | Circulation on **(A)** 200 hPa and **(B)** 500 hPa (shown as streams with wind speeds shown as shaded; units: m s^{-1}) on 0000 UTC 06 August. The hurricane symbol represents the position of Lekima near the surface, and "H" represents the anticyclonic vortex center on 200 hPa.

shortwave radiation (Dudhia, 1989) and Rapid Radiation Transfer Model (RRTM) longwave radiation parameterization scheme (Mlawer et al., 1997) are used.

The initial and boundary conditions are obtained from $1^{\circ} \times 1^{\circ}$ National Centers for Environmental Prediction/Final Analysis data (NCEP/FNL), which has 34 layers from 1,000 to 40 hPa at 6-hour intervals. The RI period of TC is from 1200 UTC 06 to 1200 UTC 08 August. The initial time of the numerical simulation is at 0000 UTC 06 August 2019. The integration lasts for 3 days from 06 to 08 August, which covers the period of RI for Lekima.

ENVIRONMENT OF LEKIMA

Lekima (2019, 09W) was first monitored as a tropical disturbance by the Joint Typhoon Warning center (JTWC) on 0600 UTC 04 August 2019. The storm strengthened and became a typhoon on 1200 UTC 06 August. At that time, the minimum central pressure was estimated to be 985 hPa. The intensity of the typhoon continued to develop. On 0600 UTC 08 August, it reached STY category with a minimum central pressure of 912 hPa and maximum wind speed of 75 m s^{-1}. The typhoon weakened slightly on 1800 UTC 08 August. **Figure 1** presents the circulations on 200 and 500 hPa at the initial time of our simulation on 0000 UTC 6 August. TC is located to the southern-east flank of the upper-level anticyclone on 200 hPa. **Figure 1B** shows that TC is mainly embedded in the cyclonic circulation on 500 hPa. And the typhoon was affected by the straight east wind located to the north flank of the typhoon on 500 hPa. The vertical structure of the anticyclone is shallow and is confined in the upper level.

The simulated track and intensity are compared against the Japan Meteorological Administration (JMA) best-track data (**Figure 2**). Generally, the simulation captures reasonably well the storm's northwestward movement. Furthermore, the intensity forecast is very close to the best track estimate. The averaged sea surface temperature from 0000 UTC 6 August to 0000 UTC 8 August is relatively high (above 29°C) which is beneficial to the development of the typhoon (**Figure 2A**). During the integration period from 0000 UTC 6 August to 0000 UTC 8 August, the central pressure of the storm fell 65 hPa within a 48-h period, which satisfies the criteria for RI for western North Pacific TCs (Wang and Zhou, 2008). With the good track and intensity prediction, the RI processes can be analyzed with detailed structure using the simulation as the proxy of the real atmosphere.

Upper-Level VWS

There is an asymmetry of Rossby waves under the vertical shear (Wang and Xie, 1996). That is, the amplitude of wave is enhanced (weakened) at the lower troposphere under easterly (westerly) shear. With this regard, the easterly shear favors a greater amplitude of wave at the lower level and thus a stronger air–sea interaction. We define the wind difference between 200 and 500 hPa as the upper-level shear. **Figure 3** presents the time evolution of the vertical profiles of the steering flows and the evolution of VWS in the vicinity of Lekima averaged within a 500-km radius centered on the storm and with the TC vortex

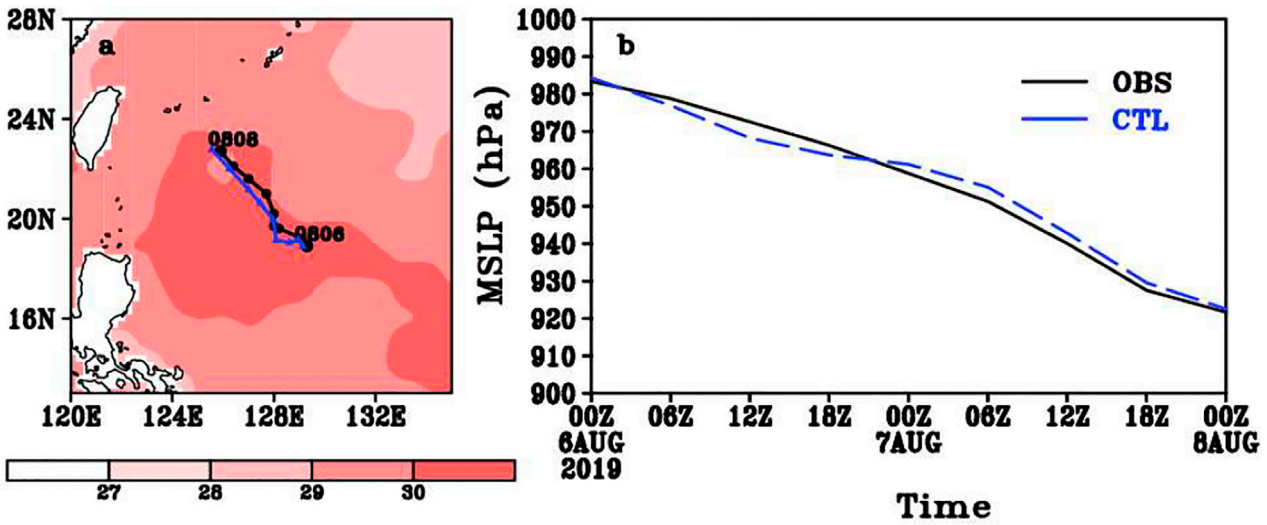

FIGURE 2 | (A) Observed and simulated track and the 2-day averaged sea surface temperature from 0000 UTC 6 to 0000 UTC 8 August (shaded; units: °C) and **(B)** the intensity of Lekima from 0000 UTC 6 to 0000 UTC 8 August 2019.

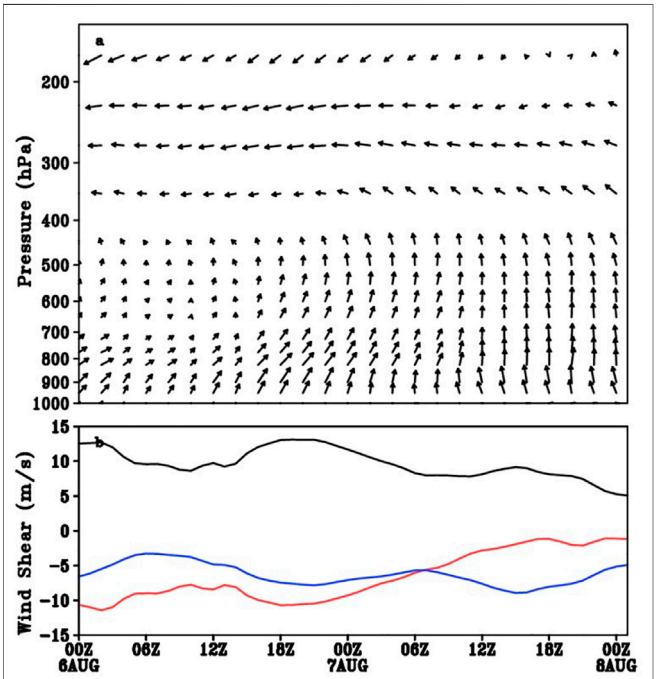

FIGURE 3 | Time evolution of the vertical profiles of **(A)** the steering flows (units: m s^{-1}) and **(B)** the wind shear (200–850 hPa; units: m s^{-1}) from 6 to 8 August. Black line is the total wind speed for the VWS, red line is the zonal component and the blue line is the meridional component of the VWS.

removed. The spatial filtering technique (Hendricks et al., 2011) was used to separate the TC-scale circulation and the large-scale circulation. Specifically, the component with wavenumber greater than 500 km is used to present the environmental flows. The initial magnitude of VWS from 850 to 200 hPa is 12 m/s, which is in the range of moderate-to-strong shear (Molinari et al., 2004; Molinari et al., 2006; Ryglicki et al., 2019). During the period of interest, the magnitude of VWS progressively decreases, albeit with some oscillations. The environmental winds change from southwesterly to southerly below about 500 hPa to nearly uniform easterly above. To further investigate the vertical structure of the VWS (not shown), the vertical profiles of the zonal components of the VWS show a prevailing easterly (westerly) wind appears at the upper (lower) level with a transition layer at about 500 hPa on 0000 UTC 06 August and 0000 UTC 07 August. The upper level VWS from 500–200 hPa is about 6 m s^{-1} and the lower level VWS from 900–500 hPa is about 4 m s^{-1}. On 0000 UTC 08 August, the easterly wind became very small at lower levels so that the VWS is mainly located in upper levels. During the first 48 simulation hours, a southerly wind appears below 350 hPa and a weak northerly wind appears up to 350 hPa. The northerly wind changed to the weak southerly wind on 0000 UTC 08 August. In short, the meridional component of the VWS is about 6 m s^{-1} during the whole integration.

What kind of synoptic weather pattern results in such upper-level VWS? To answer this question, we go back to the 200 and 500 hPa circulation presented in **Figure 1**. The anticyclone is confined in the upper level and disappears on 500 hPa. Hoskins et al. (1985) shows that the lowest vertical extent of the upper-level cyclonic potential vorticity (PV) anomaly is 800 hPa, while the lowest vertical extent of the upper-level anticyclonic PV anomaly is 300 hPa. Notice that the TC is located to the southern flank of the upper-level anticyclone. This pattern agrees well with the findings by Ryglicki et al. (2018a) and Ryglicki et al. (2018b). The authors pointed out that, the upper-level anticyclone generally creates moderate upper-level VWS, and TCs embedded in such environment likely have a potential to undergo RI. Compared with upper-level VWS, a

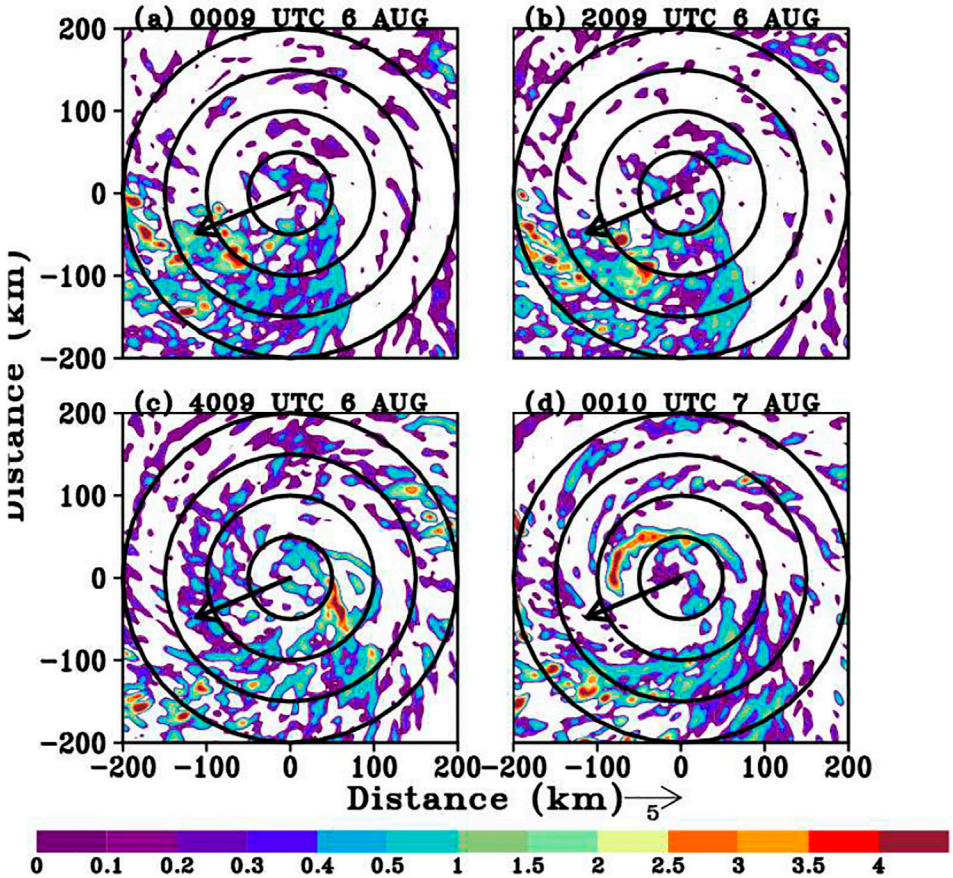

FIGURE 4 | Time evolution of the 10-km vertical velocity (shaded; units: m s^{-1}) from 0900 UTC 6 August to 1000 UTC 7 August every 20 min. Black circles are radii at every 50 km. Black arrows are the shear direction.

lower-level shear is more detrimental to TCs (Rhome et al., 2006; Zeng et al., 2010; Wang et al., 2015; Finocchio et al., 2016). Since Lekima undergoes a RI process under moderate upper-level VWS, a question arises here is what processes account for the RI of STY Lekima in the presence of the VWS? To address this, we will focus on the realignment process and the tilt-modulated convective asymmetries during the RI period.

SIMULATED RESULTS

Evolution of Convective Asymmetries

As shown in **Figure 2**, the intensity change of Lekima is fairly well captured in our numerical simulation. In this section, we examine the evolution of storm structure and convective activity during the period of the RI. In the presence of VWS, the tilted vortex generally induces asymmetric wavenumber one structure of convection. That is, a prolific convection usually occurs at the downshear-left quadrant in the Northern Hemisphere. To illustrate such asymmetric feature, **Figure 4** displays the distribution of the convection represented by the simulated vertical velocity from 0900 UTC 6 August to 1000 UTC 7 August every 20 min. The CBs are defined as the cells with vertical velocity greater than 2 m s^{-1} from 0.5 to 10 km in each level. Here the vertical velocity field at the height of 10 km is selected to represent the CBs. The VWS is mainly the northeast easterly vertical wind shear. The simulated convective asymmetries are evident, with more extensive, more active convection located to the southwest of the storm center, and the convection moves inward and counterclockwise with time. **Figure 5** presents the simulated hourly rainfall and the satellite-observed infrared brightness temperatures for comparison during the simulated RI period. The asymmetry distribution of the hourly rainfall is located in the downshear-left quadrant near the storm center at the simulation of 12 h. The distribution of the hourly rainfall becomes more symmetric with time. Initially, the strong convective cloud band represented by the coldest temperature occurs to the southwest section of TC center. During the period of interest, the strongest convection is expanded to the upshear side, and the eyewall cloud becomes more symmetric. Meanwhile, the inner cloud band within 200 km from the center of the TC extends southeastward, and it corresponds with the outflow at the top; both move upshear flank with time. In general, the simulated asymmetry agrees fairly well with the satellite-observed infrared brightness temperatures (**Figures 5D–F**).

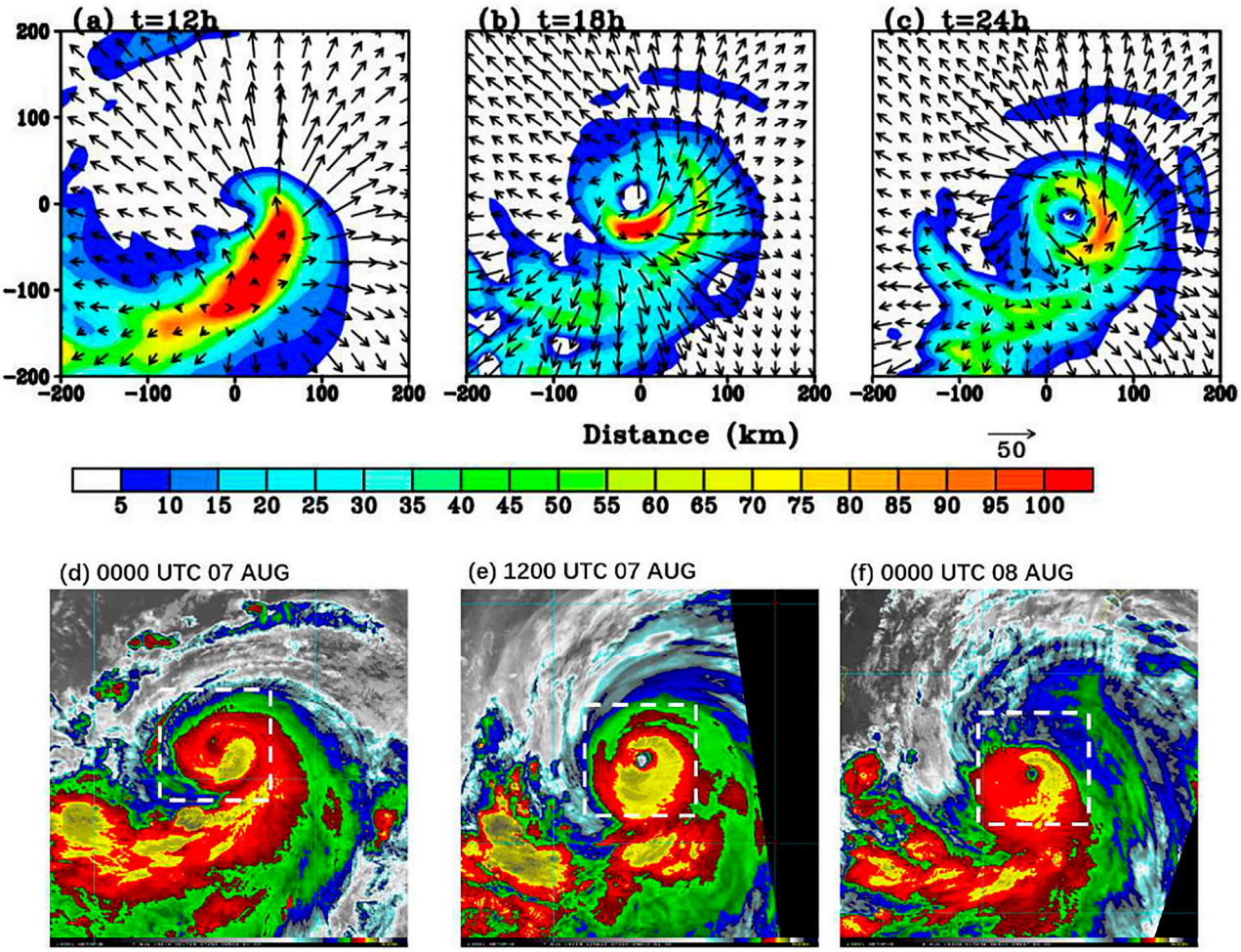

FIGURE 5 | Upper panels: Snapshot at 12, 18, and 24 h of the simulated hourly rainfall and the outflow (black vectors; units: m s^{-1}) at 17 km starting on 0000 UTC 6 August. Lower panels: the time evolution of the satellite-observed infrared brightness temperatures from 0000 UTC 7 August to 0000 UTC 8 August on the NOAA website. The white dashed box in the bottom panels is the 200 × 200 km area centered by the TC, covering the same area as in the top panels.

The deep convection represented by the CBs is akin to the so-called vortical hot towers (VHTs) described in Hendricks et al. (2004) and Montgomery et al. (2006). During the early development stage of Lekima (i.e., 1200 UTC 06 August 2019), the convective asymmetry originates over the southwest sector to the storm center. With times, the most active convection moves anticlockwise, and approaches to east flank of the storm (**Figure 5**). This evolution feature bears many similarities as previous studies (Ryglicki et al., 2018a; Ryglicki et al., 2018b; Li et al., 2020), indicating that an inward-spiraling inner cloud band moves to upshear flank to form the eyewall cloud. This process agrees with Moon and Nolan (2010), in which they proposed a hypothesis that inner rainbands are simply convective clouds advected by the rapidly rotating TC wind, and then likely deformed into spiral shapes. Through axisymmetrization, the entity likely provides a source of vorticity for the developing inner core.

In short, the simulation demonstrates that in the presence of the VWS, strong CBs occur at the left-downshear section and then are transported cyclonically into the upshear section to form the eyewall. During this period, the magnitude of VWS is gradually reduced (**Figure 3**). In response to the shear reduction, the tilting of vortex is reduced and becomes almost vertically realigned. To demonstrate this feature, **Figure 6** displays the horizontal distribution of low and upper-level circulations in the simulation. Initially, there is an obvious displacement between the lower-level and upper-level circulation centers (i.e., 00 UTC 06 August), with the upper-level circulation center located about 80 km southwest of the lower-level center. During the period from 6 to 7 August, along with the reduction of VWS, the horizontal displacement between mid- and upper-level centers becomes quite small (i.e., less than 10 km), indicating a vertical realignment process.

Ryglicki et al. (2018a) and Ryglicki et al. (2018b) pointed out that, while the TCA moves towards upshear flank, the cumulative effect of the continuous convective events is to push the upper-level upshear environmental winds away from the TC center. As a result, this dynamical process reduces the local wind shear and

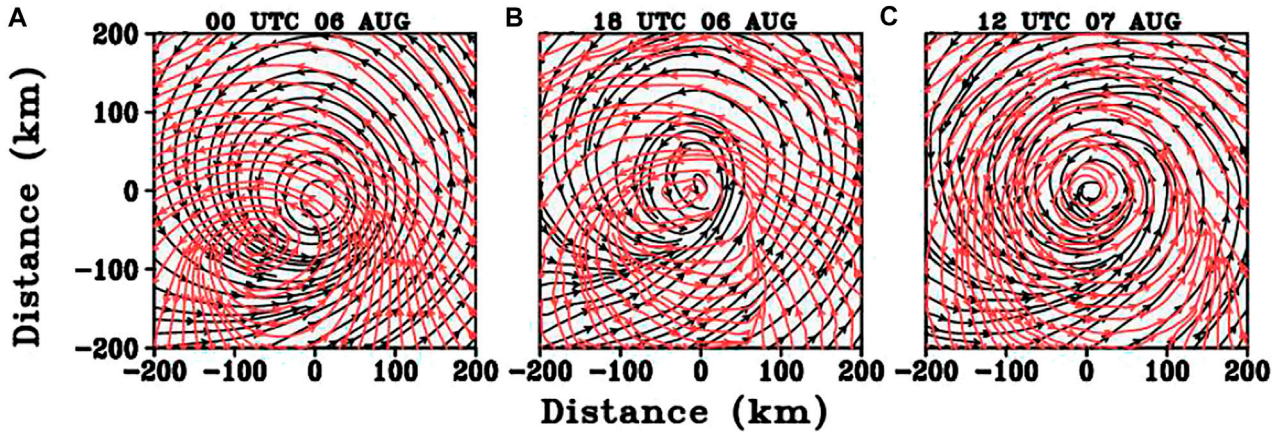

FIGURE 6 | Horizontal distribution of low (0.25-km; black stream) and upper (10-km; red stream) level cyclonic circulations on 0000 UTC 06, 1800 UTC 06, and 1200 UTC 07 August. The (0,0) represents the center of the low-level cyclonic circulation.

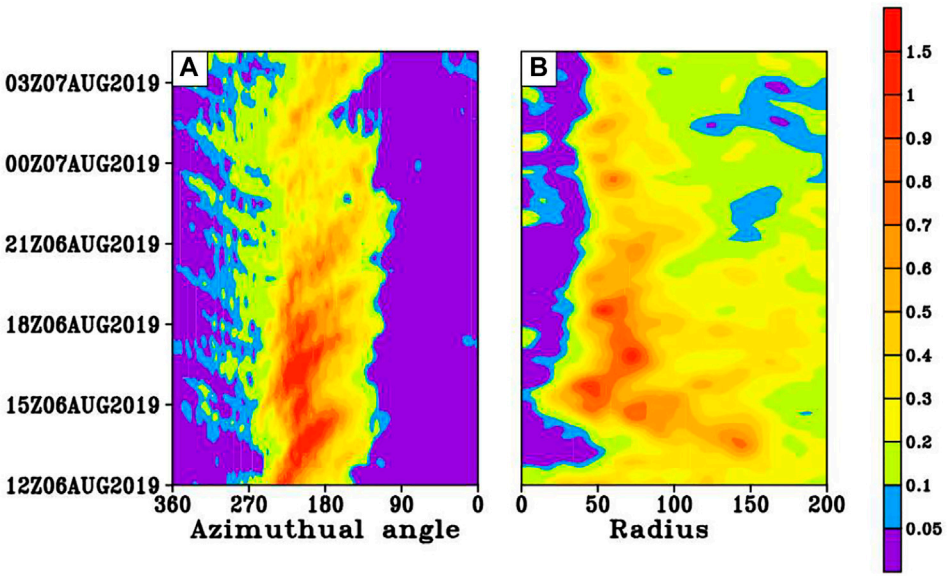

FIGURE 7 | Time revolution of the vertical velocity (m s^{-1}) at 10-km, **(A)** radially averaged from 60 to 180 km and **(B)** azimuthally averaged from 90° to 270°. Azimuth angles are math convention, such that the azimuthal angle 0° is defined as north (right of shear), 90° is defined as east (up shear), 180° represents southward (left of shear), and 270° represents westward (down shear).

helps vortex realignment. To illustrate the evolution features of TCA, **Figure 7A** displays the time-azimuthal cross section of vertical velocity averaged within the radius of 60–180 km. The azimuthal angle 0° is defined here as due north, and 180° represents southward since it rotates clockwise. It is apparent that the strong vertical motion origins constantly around the azimuthal angle of 270° (downshear flank) and then propagates counterclockwise to about 90° (upshear flank). **Figure 7B** presents the time-radius cross section of the vertical velocity azimuthally averaged from 90° to 270°. It shows that strong ascending motion moves radially inward from 1300 UTC 6 August to 1500 UTC 6 August and then stays close to the RMW, reflecting that the CBs moves closer to the RMW before and during RI.

In short, our simulation shows the evolution characteristics of Lekima in which periodically generated asymmetric convective cloud bands are wrapped cyclonically into the upshear flank of the eyewall. To reveal their possible roles on the RI, Fourier decomposition is used to extract the azimuthal wavenumber-1 component of vertical mass fluxes at 17 km from 0800 UTC 06 August to 1900 UTC 06 August (not shown). Clearly, the asymmetry maximum is initially located in the downshear-left quadrant, which is outside the RMW (about 60 km). With time, the maximum shows a cyclonic movement and approaches the

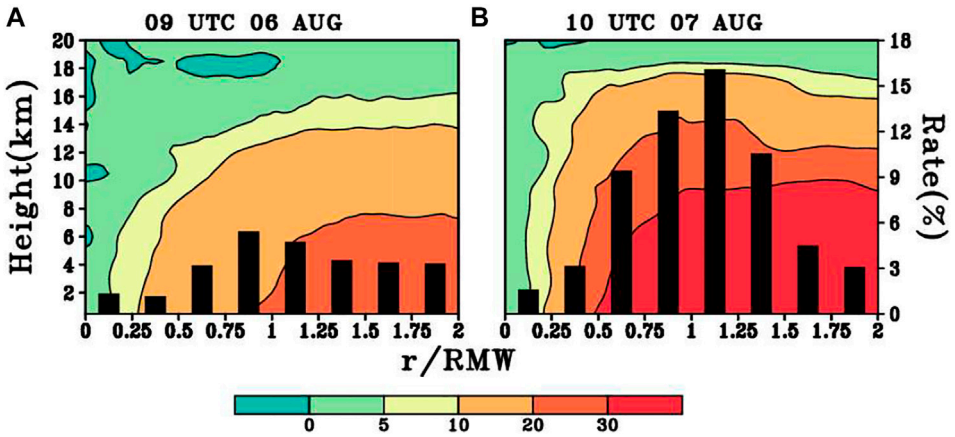

FIGURE 8 | Radial distribution of CBs, shown as which shows the percentage of the CBs at each radial distance (bar; $w > 2$ m s^{-1}; units: %) and the tangential wind (shaded; units: m s^{-1}) with respect to the RMW on 0900 UTC 06 and 1000 UTC 07 August.

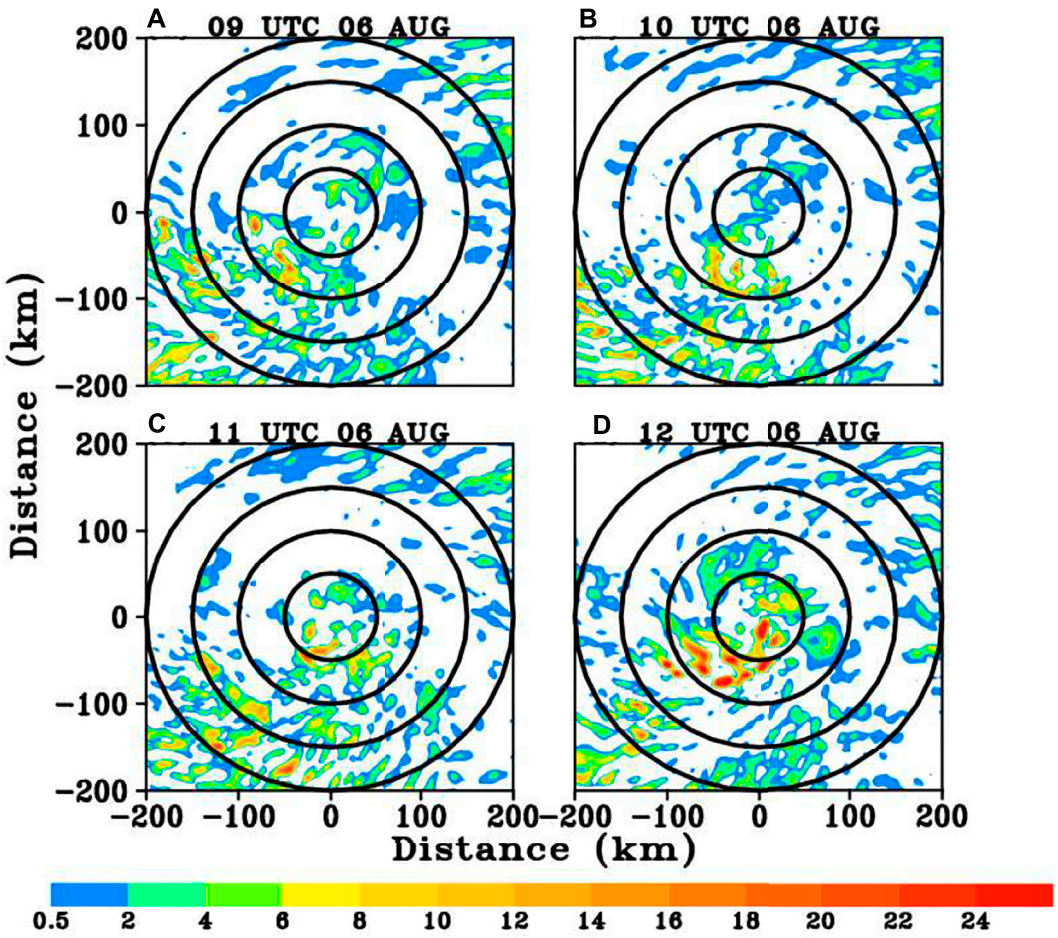

FIGURE 9 | Time evolution of radial eddy vorticity flux ($-V_r'\zeta'$, shading; units: 1×10^{-3}, m s^{-2}) at 17-km from 0900 UTC to 1200 UTC 06 August.

RMW. This reflects the progressive cyclonic precession of the convective complex and more active convection near or within the inertially stable TC core for TC intensification, consistent with previous studies (Nolan et al., 2007; Vigh and Schubert, 2009; Finocchio et al., 2016). By comparing the composites for the relatively early onset of RI members and the late onset of RI

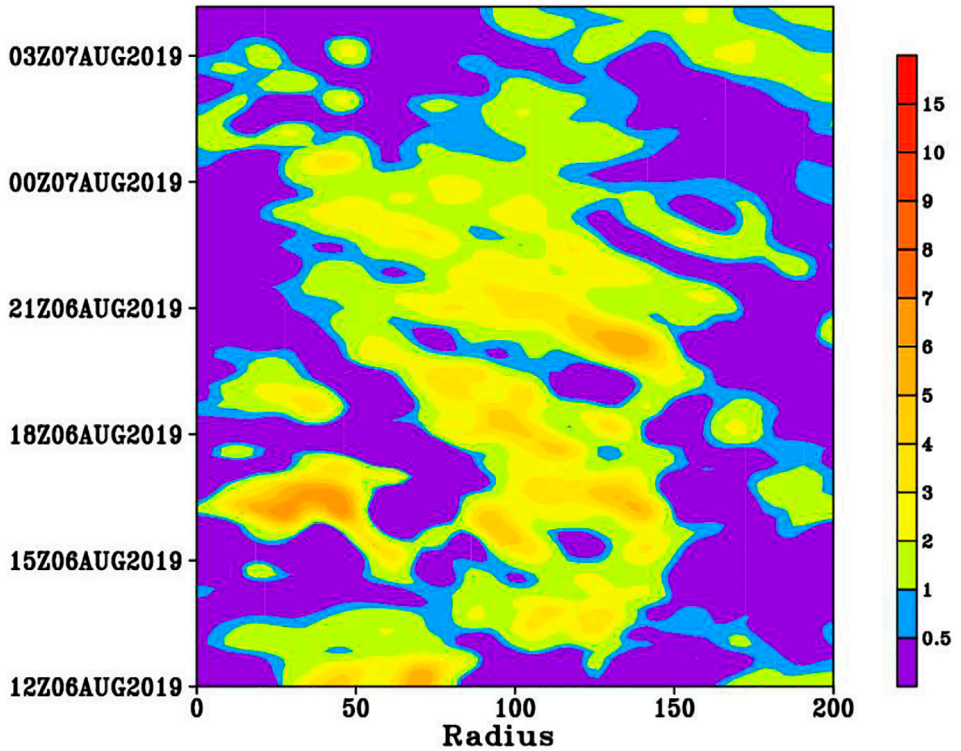

FIGURE 10 | Time-radius cross section of radial eddy vorticity flux ($-V_r'\zeta'$, shading units: 1×10^{-3}, m s^{-2}) at 17-km from 1200 UTC 06 to 0400 UTC 07 August.

members, Li et al. (2020) suggested the early RI members with high environmental moisture and weak ventilation show the asymmetric convection develops actively and moves from the downshear side to the inner core to reduce the tilting of the TC. However, the late RI members under the stronger VWS show larger ventilation that is not conductive to TC intensity.

From a physical perspective, a larger vertical mass flux implies more pronounced diabatic heating. Furthermore, the closer the diabatic heating to the RMW where the inertial stability is the largest, the larger the conversion rate of heating to the kinetic energy. To understand this dynamic and thermodynamic aspect, the radial distributions of CBs relative to the RMW are plotted at two given times from our simulations (**Figure 8**). The radial distribution of CBs shows the percentage of the CBs at each radial distance normalized by the RMW at the height of 1.5 km. Since the RMW evolves with time, the CBs distribution is displayed with the *x*-axis normalized by the corresponding RMW at each time snapshot. Notice that the radial distributions of CBs exhibit a marked difference with respect to RMW between these two times. At the early stage (i.e., 0900 UTC 06 August), the radial distribution of strong convection mostly stays away the RMW. With time, CBs near the RMW increase, and start to move inward and closer to the RMW as shown on 1000 UTC 07 August. This agrees with previous studies (Rogers et al., 2016; Hazelton et al., 2017), namely, CBs need to occur inside, not outside the RMW, in sufficient numbers for genesis and intensification (Braun, 2013).

The axisymmetrization processes associated with rotating convective updrafts in and around the developing eyewall region have been shown to contribute to an enhanced secondary circulation (Montgomery et al., 2014; Montgomery and Smith, 2014; Smith et al., 2017; Chen et al., 2018). To further assess the dynamical influences of these eddies on the TC intensification, we calculate the term $-V_r'\zeta'$ at 17 km (**Figure 9**), where V_r' is radial inflow anomaly and ζ' is the vorticity anomaly. Dynamically, the positive value implies that the eddies will enhance the mean circulation. These eddies are defined as the positive cyclonical vorticity. The positive vertical velocity is mainly located in the downshear-left quadrant and moves to the upshear quadrant (**Figure 4**). As expected, the spatial pattern clearly shows the asymmetric structure with the positive value dominated in the downshear-left section. **Figure 10** displays the time-radius cross section of eddy vorticity fluxes at the height of 17 km. Once again, the positive value exhibits consistent and periodic inward propagation, coinciding with the inward propagation of asymmetric convective band. Consequently, the positive value helps spin up the upper-level inner-core circulation.

To summarize, under moderate upper-level easterly VWS, TC exhibits a wavenumber-one TCA indicated by strong upward motion to the downshear-left side of the storm. This tilting-induced convective asymmetry, which resembles the inner convective bands (ICBs), is then transported and/or wrapped inwards to the upshear quadrant to form an eyewall. Along with the continuous development of inward-penetrating ICBs, the vortex starts to undergo vertical realignment. Since the deep

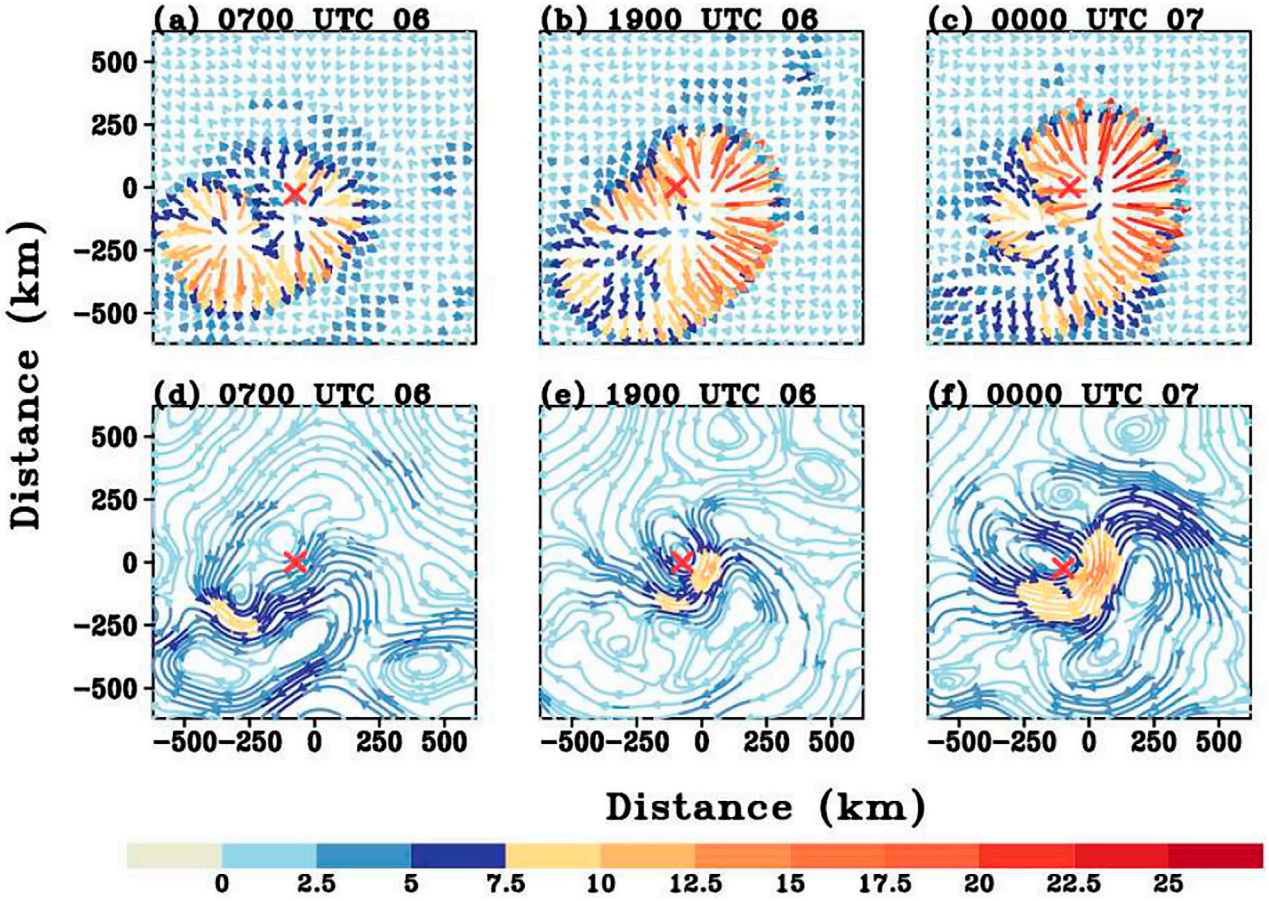

FIGURE 11 | Time evolution of the divergent winds (top panels; units: m s^{-1}) and rotational winds (bottom panels; units: m s^{-1}) at 17-km height from 0700 UTC 6 August to 0000 UTC 7 August. Red × is the low-level center of the storm.

CBs are the nature source to drive TC outflow, we will examine the evolution of TC outflow structure in the following section.

Evolution of Outflow Structure

For a TC with RI, one pronounced feature is a strong upper-level outflow jet with an open circulation (Merrill, 1988). Generally, a strong outflow channel will efficiently ventilate the mass from storm center, resulting in a rapid falling of sea-level pressure. Previous studies suggested that outflow serves to divert and to block the environmental flow at upper levels (Elsberry and Jeffries, 1996; Ryglicki et al., 2019). Under favorable circumstances, the outflow could reduce VWS in the upper levels near the storm, allowing it to intensify.

Following Finocchio et al. (2016), the upper-level horizontal circulation is decomposed into the divergent and rotational components, respectively. **Figure 11** presents the time evolution of divergent wind (top panels) and rotational wind (bottom panels) at the height of 17 km. Initially, two divergent flows occur at this level: one is close to the storm center and the other is located to the downshear-left region, coinciding with the TCA. With time, the latter appears to approach the vortex center so that the strongest divergent winds are concentrated in the upshear flank. The repeated generation of TCA moving cyclonically and forming an eyewall is speculated that this process greatly enhances the upper divergent flows. The enhanced divergent flow acts as an important source of the blocking to the environmental flow and thus the reduction of VWS (Ryglicki et al., 2018a, Ryglicki et al., 2018b). Meanwhile, the rotational wind is reinforced as part of an anticyclonic circulation to the eastern flank of the storm center. Accordingly, an open outflow channel is established.

In the presence of outflow channels in the vicinity of the TC, it is reasonable to expect less energy expenditures since the outflow channels can provide low inertial stability so that minimal work is required to vent the outflow against the radial pressure gradient. Furthermore, as the outflow channels extend outward to a wider area, it may change the environmental conditions and thus their effect on core convection and tropical cyclone intensity. We will examine the relationship of the ambient upper-level outflow and the organization of TC convective entities. Two possible mechanisms may account for their interactions. On the one hand, the organized outflow plays an important role in sustaining the inner-core deep convection in developing TCs. It stands to reason that, as a branch of the secondary circulation,

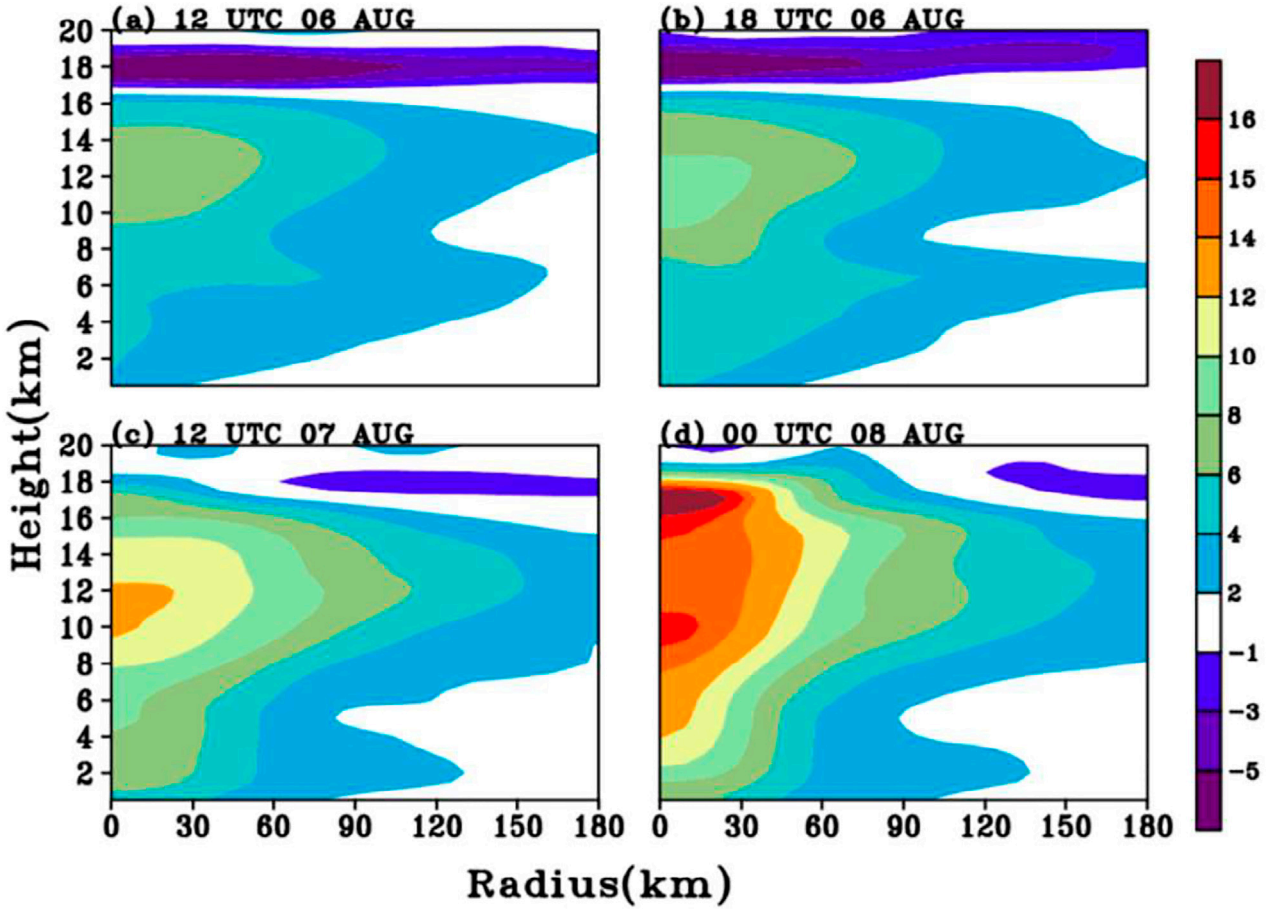

FIGURE 12 | Time evolution of the radius-height cross sections of the azimuthal mean temperature anomaly (units: K) from 1200 UTC 6 August to 0000 UTC 8 August.

strong outflow would curtail subsidence adjacent to the updrafts in the storm core. As such, this ventilation away from the core would promote compensating subsidence farther away from TC center (Pratt and Evans, 2009). On the other hand, this setup promotes a prolific deep convection, which is the natural source to drive the outflow. With these regards, it is important to understand how the outflow channel influences the convective activity by modulating the environmental conditions. To address this question, we take a close look at the storm's structure at upper levels.

Figure 12 displays the radius-height cross sections of the azimuthal mean temperature anomaly at four snapshots during the RI period. The temperature anomaly is relative to the area average between 300 and 500 km away from the storm center at each level. In early stage, there is an intense cold anomaly at the upper troposphere just above 17 km (**Figures 12A,B**). With time, this cold anomaly extends outward and gradually weakens and is replaced by the warm anomaly when the storm intensifies. Along with the rapid intensification, both the magnitude and height of the warm core increase. By 0000 UTC 8 August, the warm core is well established throughout the troposphere (**Figure 12D**). This is consistent with the finding by Rivoire et al. (2016).

Using temperature retrievals from the remote sensing platforms, Rivoire et al. (2016) examined the evolution of the fine-scale temperature structure within TCs. The authors found that the convective structure evolves highly asymmetrically with respect to the lifetime maximum intensity (LMI). More specifically, relative to the far-field structure, tropopause-level cooling occurs before a tropospheric TC warm core is established. In the present study, we also identify similar evolution feature. That is, the tropopause-level cooling precedes the warm core signal and move away from the storm during the RI period. Rogers et al. (2013) found that, the complex relation between the tropopause level cooling and the convective bursts is beneficial to intensifying TCs. We will investigate the possible processes leading to such cold anomalies.

Physically, both the long wave radiation due to the cloud anvils and the adiabatic cooling associated with deep CBs can contribute to the upper-level cooling. It is likely that, when the upper-level outflow jet channel is established and extends to a broader horizontal area, it can carry the hydrometers away from the storm center and forms a large cloud anvil. Gao et al. (2020) suggested that, compared with lower-layer VWS, upper-layer VWS is apt to produce stronger upper-level outflow in the downshear-left quadrant. This stronger

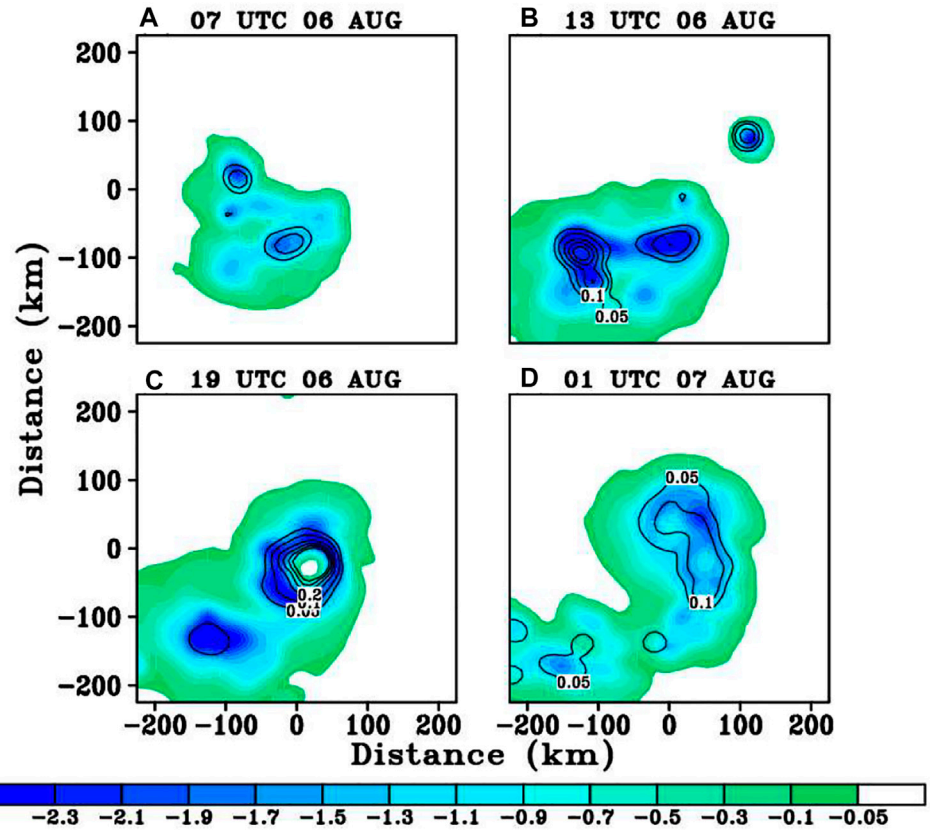

FIGURE 13 | Time evolution of the hydrometers (contour; units: g/kg) and temperature tendency due to radiation (Q_r, shaded; units: K/h) at 18-km from 0700 UTC 06 to 0100 UTC on 07 August.

outflow transports more water vapor radially outward from the inner core to the outer core in the downshear-left quadrant, resulting an organized stratiform cloud in the outer rainbands. The cloud avail will bring about a cooling due to the longwave radiation process. For further understanding, the upper-level hydrometers and temperature tendency due to radiation (Q_r) at 18 km are examined in **Figure 13**. As anticipated, there exists a large portion of hydrometers (mostly are ice and snow) in the downshear-left quadrant, since the outflow channel goes southwestward. Furthermore, there is an asymmetric pattern in Q_r with the minimum located in the downshear-left quadrant. These radiative patterns are consistent with the signatures of thick anvils.

Using a cloud-resolving model, Kuang and Hartmann (2007) demonstrated that convection has a cooling effect in the tropopause layer that significantly affects the thermal structure of the environment. In particular, the cold anomaly in the tropopause layer is found to be strongly tied to the convective cooling maximum. Here we calculate the dynamical cooling effect, which is formulated as follows:

$$Q_{dyn} = -\overline{w}\left(\partial_z T + \frac{g}{C_p}\right), \quad (1)$$

where $\overline{w}$ is the vertical velocity, T is temperature, C_p is the specific heat of dry air at constant pressure, g is the gravity constant, $-\partial_z T$ represents the environmental lapse rate (γ), and $\frac{g}{C_p}$ is the dry adiabatic lapse rate (γ_d).

Figure 14 presents the time evolution of the averaged 6 h radius-height cross section of the azimuthally averaged dynamical cooling effect (Q_{dyn}), the temperature tendency due to the radiation (Q_r), and the diabatic heating due to the microphysics (Q_{ht}) and sum of the three terms from the height of 15–20 km from 0700 UTC 06 to 1300 UTC 06, 1300 UTC 06 to 1900 UTC 06, and 1900 UTC 06 to 0100 UTC 07 August. There is a dynamical cooling corresponding to the deep CBs. Conversely, the sinking motion may produce a dynamical warming in association with a warm anomaly. In the tropopause layer, there is indeed pronounced dynamical cooling at the storm center, which is closely associated with the updrafts of the deep CBs. The dynamical cooling by the inner updrafts is gradually increasing from 0700 UTC 06 to 0100 UTC 07 August, and the adiabatic cooling extends outward from the inner core with time. However, the microphysics heating remains basically stable. It is possible that, due to the scarcity of upper-level moisture supplies, the diabatic heating due to the microphysics cannot offset the adiabatic cooling and thus partially accounts for the upper-level cooling anomalies. Furthermore, the upper-level thermodynamical structure will modify

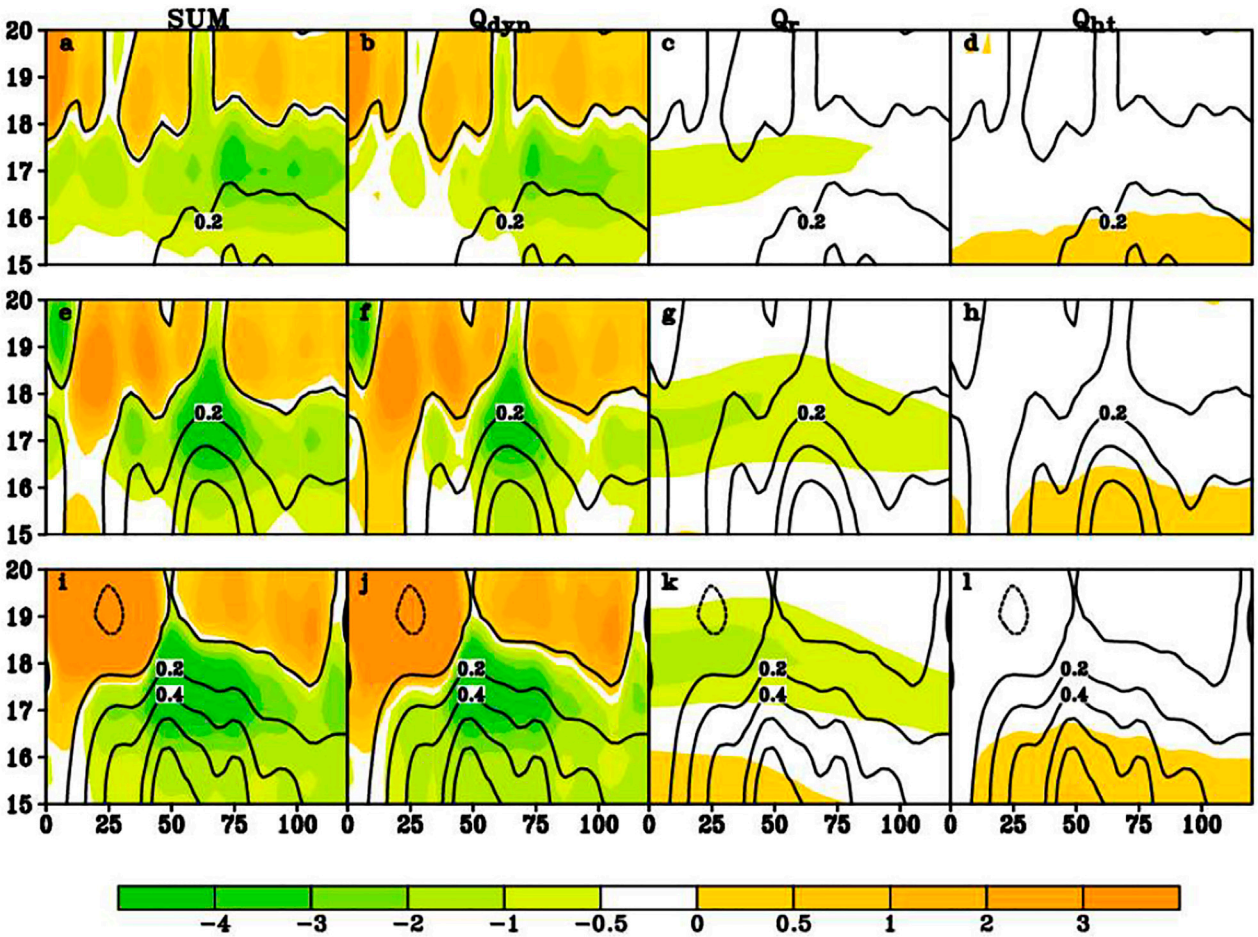

FIGURE 14 | Six-hour averaged radius-height cross section of the azimuthally averaged thermodynamical structure and the vertical velocity (contour; units: m s-1) in the inner core between 15 and 20 km height from 0700 UTC to 1300 UTC 06 Aug (the first row), 1300 UTC to 1900 UTC 06 Aug (the second row), and 1900 UTC 06 to 0100 UTC 07 August (the third row). The first column: sum of the three terms to the right (shaded; units: °K/h); The second column: dynamical cooling effect (Q_{dyn}) (shaded; units: K/h); the third column: temperature tendency due to radiation (Q_r) (shaded; units: K/h); the fourth column: diabatic heating due to microphysics (Q_{ht}) (shaded; units: K/h).

the static stability, which is possibly the primary driver of the invigoration of deep convection (Willoughby, 1998; Ruppert and Hohenegger, 2018), namely, cold anomalies at the tropopause locally destabilize the atmosphere, which enhances the deep convection and thus promote the development of outflow channels.

In short, the cold anomalies precede the establishment of a strong warm core, and this might reinforce the secondary circulation and indirectly stiffen the vortex against VWS. Recall that the strong deep CBs are mainly located to the downshear-left section, collocated with the outflow channel. To better understand the origin of convective updrafts, we now calculate the vertical velocity tendency due to the local buoyancy production, which is defined as follows:

$$\frac{dw}{dt} = g\frac{T'}{\overline{T}}, \tag{2}$$

where the bar represents the azimuthal-mean, and the prime indicates the asymmetric component deviated from the azimuthally averaged. **Figure 15** presents the snapshots of spatial pattern of acceleration of vertical velocity due to the buoyancy. The largest vertical accelerations are confined at the southwestern flank of the storm center, where largely underneath the strongest upper-level cooling anomalies (**Figure 13**). To summarize, the upper-level thermal structure has shown a modulating effect on the TC intensification. However, the detailed underlying processes are less apparent. This interesting topic awaits for further studies.

CONCLUSION AND DISCUSSION

Finocchio et al. (2016) showed that, as with many other studies, the vertical wind shear (VWS) is in general not favorable for the TC intensification. However, the upper-level VWS has slightly less influence on the TC intensity than the low-level VWS. Super typhoon Lekima (2019) in the western North Pacific went through RI under an upper-

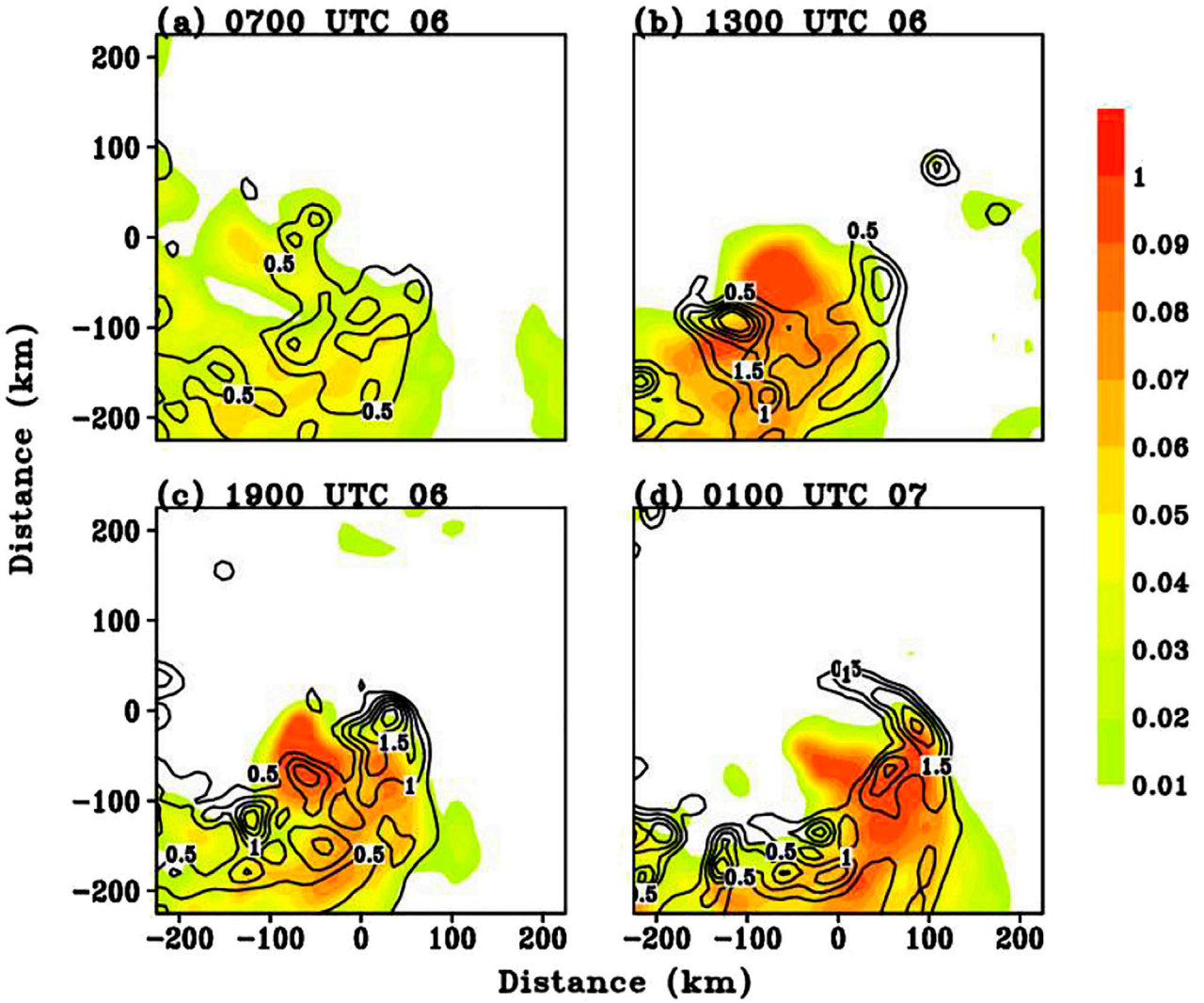

FIGURE 15 | Evolution of the effective buoyancy acceleration (shaded; units: m s^{-2}) and vertical velocity (contour; m s^{-1}) at 10-km from 0700 UTC 6 August to 0100 UTC 7 August.

level VWS, defined between 500 and 200 hPa. In this study, a comprehensive analysis of Lekima is conducted using a numerical simulation. The focus is on the inner convection process and its relation with the cold anomalies at the tropopause under the upper level VWS during the RI process of Lekima. The main findings are summarized as the follows:

1) Under moderate upper-level easterly VWS, a wavenumber-one convective asymmetry indicated by strong upward motion and large reflectivity occur to the downshear-left side of the storm center in the initial stage. This tilting-induced convective asymmetry, constituted by ICBs, is then transported cyclonically to the upshear quadrant and wraps around the storm center and becomes as part of the eyewall. The upward motion is further enhanced, particularly in the upshear flank, to create upper-level divergent flow. As such, the establishment of outflow divergent flow acts against the environmental flow to reduce the VWS. The vortex starts to undergo vertical realignment. Accompanied with the synchronization between the mid- and low-level circulations, there is the repeating development of inward-penetrating ICBs that eventually forms the eyewall.
2) In turn, upper-level conditions exert a modulating effect on the TC intensification, specifically the development of an outflow channel that evacuates mass from the storm center. The organized outflow plays an important role in sustaining the inner core deep convection via modulating the upper-level thermal structure. In the early stage, cold anomalies are generated in the tropopause layer, mainly due to the adiabatic cooling by the deep ICBs and radiative process associated with the cloud anvil. Physically, cold anomalies at the tropopause locally destabilize the atmosphere, enhance the deep convection, and thus promote the development of outflow

channels. The eyewall cloud continues to develop episodically through this process as it wrapped around the storm.

Our simulation reveals that the development of the eyewall occurred as a convective band wrapped inward from the downshear-left sector, which is closely related to the vertical realignment of the sheared vortex, in particular the alignment vertically over the upshear quadrants. This process suggests a different pathway of TC RI from the one described by Molinari et al. (2006), in which TC intensification under a sheared environment can be promoted when a TC vortex undergoes a "downshear reformation" to suppress the ventilation effect. Specifically, a new vortex is generated by the downshear convection, becomes the new storm center, and then intensifies through the combination of surface enthalpy fluxes and the absence of penetrative downshear-right downdrafts. It is argued that this intensification process was set into motion by the vertical wind shear in the presence of an environment with upward motion forced by the approaching upper tropospheric trough.

Finocchio et al. (2016) indicates the complexity of different VWS patterns, and different convective asymmetric structures likely result in different outcomes for the intensification of a TC. To gain better understanding, simulations with different initial vortex structures and environmental conditions will be conducted in the future. For instance, the different structure of initial vortices (i.e., sizes and vertical depths) may provide sources of uncertainty for RI, since the vertical realignment will depend on these size factors. Furthermore, the heterogeneous environmental moisture conditions are also important for the asymmetric convective structure. More future works will focus on these topics.

DATA AVAILABILITY STATEMENT

The original contributions presented in the study are included in the article/Supplementary Material; further inquiries can be directed to the corresponding author.

AUTHOR CONTRIBUTIONS

QH and XG designed and executed field experiments. XG and MP analyzed data and wrote the article.

FUNDING

This work was jointly sponsored by the National Natural Science Foundation of China (42088101; 42175003) and the Science and Technology Innovation Project of Ningbo (Grant No. 2019B10025). The numerical calculations are performed on the supercomputing system in the Supercomputing Center of Nanjing University of Information Science & Technology.

REFERENCES

Bhalachandran, S., Chavas, D. R., Marks, F. D., Jr., Dubey, S., Shreevastava, A., and Krishnamurti, T. N. (2020). Characterizing the Energetics of Vortex-Scale and Sub-vortex-scale Asymmetries during Tropical Cyclone Rapid Intensity Changes. *J. Atmos. Sci.* 77, 315–336. doi:10.1175/jas-d-19-0067.1

Braun, S. A., Kakar, R., Zipser, E., Heymsfield, G., Albers, C., Brown, S., et al. (2013). NASA's Genesis and Rapid Intensification Processes (GRIP) Field Experiment. *Bull. Amer. Meteorol. Soc.* 94, 345–363. doi:10.1175/bams-d-11-00232.1

Chen, H., and Gopalakrishnan, S. G. (2015). A Study on the Asymmetric Rapid Intensification of Hurricane Earl (2010) Using the HWRF System. *J. Atmos. Sci.* 72, 531–550. doi:10.1175/jas-d-14-0097.1

Chen, H., and Zhang, D.-L. (2013). On the Rapid Intensification of Hurricane Wilma (2005). Part II: Convective Bursts and the Upper-Level Warm Core. *J. Atmos. Sci.* 70, 146–162. doi:10.1175/jas-d-12-062.1

Chen, X., Wang, Y., Fang, J., and Xue, M. (2018). A Numerical Study on Rapid Intensification of Typhoon Vicente (2012) in the South China Sea. Part II: Roles of Inner-Core Processes. *J. Atmos. Sci.* 75, 235–255. doi:10.1175/jas-d-17-0129.1

Chen, X., Wang, Y., Zhao, K., and Wu, D. (2017). A Numerical Study on Rapid Intensification of Typhoon Vicente (2012) in the South China Sea. Part I: Verification of Simulation, Storm-Scale Evolution, and Environmental Contribution. *Mon. Wea. Rev.* 145, 877–898. doi:10.1175/mwr-d-16-0147.1

Corbosiero, K. L., and Molinari, J. (2002). The Effects of Vertical Wind Shear on the Distribution of Convection in Tropical Cyclones. *Mon. Wea. Rev.* 130, 2110–2123. doi:10.1175/1520-0493(2002)130<2110:teovws>2.0.co;2

Dai, H., Zhao, K., Li, Q., Lee, W.-C., Ming, J., and Zhou, A. (2021). Quasi-periodic Intensification of Convective Asymmetries in the Outer Eyewall of Typhoon Lekima (2019). *Geophys. Res. Lett.* 48, e2020GL091633. doi:10.1029/2020gl091633

Davis, C. A., Wang, W., Chen, S. S., Chen, Y., Corbosiero, K., DeMaria, M., et al. (2008). Prediction of Landfalling Hurricanes with the Advanced Hurricane WRF Model. *Mon. Wea. Rev.* 136 (6), 1990–2005. doi:10.1175/2007mwr2085.1

DeMaria, M., Sampson, C. R., Knaff, J. A., and Musgrave, K. D. (2014). Is Tropical Cyclone Intensity Guidance Improving?. *Bull. Amer. Meteorol. Soc.* 95, 387–398. doi:10.1175/bams-d-12-00240.1

Dudhia, J. (1989). Numerical Study of Convection Observed during the Winter Monsoon Experiment Using a Mesoscale Two-Dimensional Model. *J. Atmos. Sci.* 46, 3077–3107. doi:10.1175/1520-0469(1989)046<3077:nsocod>2.0.co;2

Elsberry, R. L., and Jeffries, R. A. (1996). Vertical Wind Shear Influences on Tropical Cyclone Formation and Intensification during TCM-92 and TCM-93. *Mon. Wea. Rev.* 124, 1374–1387. doi:10.1175/1520-0493(1996)124<1374:vwsiot>2.0.co;2

Elsberry, R. L., Lambert, T. D. B., and Boothe, M. A. (2007). Accuracy of Atlantic and Eastern North Pacific Tropical Cyclone Intensity Forecast Guidance. *Wea. Forecast.* 22, 747–762. doi:10.1175/waf1015.1

Emanuel, K., DesAutels, C., Holloway, C., and Korty, R. (2004). Environmental Control of Tropical Cyclone Intensity. *J. Atmos. Sci.* 61, 843–858. doi:10.1175/1520-0469(2004)061<0843:ecotci>2.0.co;2

Finocchio, P. M., Majumdar, S. J., Nolan, D. S., and Iskandarani, M. (2016). Idealized Tropical Cyclone Responses to the Height and Depth of Environmental Vertical Wind Shear. *Mon. Wea. Rev.* 144, 2155–2175. doi:10.1175/mwr-d-15-0320.1

Frank, W. M., and Ritchie, E. A. (2001). Effects of Vertical Wind Shear on the Intensity and Structure of Numerically Simulated Hurricanes. *Mon. Wea. Rev.* 129, 2249–2269. doi:10.1175/1520-0493(2001)129<2249:eovwso>2.0.co;2

Gao, Q., Li, Q., and Dai, Y. (2020). Characteristics of the Outer Rainband Stratiform Sector in Numerically Simulated Tropical Cyclones: Lower-Layer Shear versus Upper-Layer Shear. *Adv. Atmos. Sci.* 37, 399–419. doi:10.1007/s00376-020-9202-y

Ge, X., Li, T., and Peng, M. (2013). Effects of Vertical Shears and Midlevel Dry Air on Tropical Cyclone Developments*. *J. Atmos. Sci.* 70, 3859–3875. doi:10.1175/jas-d-13-066.1

Gu, J.-F., Tan, Z.-M., and Qiu, X. (2015). Effects of Vertical Wind Shear on Inner-Core Thermodynamics of an Idealized Simulated Tropical Cyclone. *J. Atmos. Sci.* 72, 511–530. doi:10.1175/jas-d-14-0050.1

Hazelton, A. T., Rogers, R. F., and Hart, R. E. (2017). Analyzing Simulated Convective Bursts in Two Atlantic Hurricanes. Part I: Burst Formation and Development. *Mon. Wea. Rev.* 145, 3073–3094. doi:10.1175/mwr-d-16-0267.1

Hendricks, E. A., Montgomery, M. T., and Davis, C. A. (2004). The Role of "Vortical" Hot Towers in the Formation of Tropical Cyclone Diana (1984). *J. Atmos. Sci.* 61, 1209–1232. doi:10.1175/1520-0469(2004)061<1209:trovht>2.0.co;2

Hendricks, E. A., Peng, M. S., Ge, X., and Li, T. (2011). Performance of a Dynamic Initialization Scheme in the Coupled Ocean-Atmosphere Mesoscale Prediction System for Tropical Cyclones (COAMPS-TC). *Wea. Forecast.* 26, 650–663. doi:10.1175/waf-d-10-05051.1

Hoskins, B. J., McIntyre, M. E., and Robertson, A. W. (1985). On the Use and Significance of Isentropic Potential Vorticity Maps. *Quart. J. Roy. Meteorol. Soc.* 111, 877–946.

Kain, J., and Fritsch, J. M. (1993). "Convective Parameterization for Mesoscale Models: The Kain-Fritsch Scheme," in *The Representation of Cumulus Convection in Numerical Models*. Meteor. Monographs, 24. Editors K. A. Emanuel and D. J. Raymond (Boston, MA: American. Meteorological. Society), 246.

Kanada, S., and Wada, A. (2015). Numerical Study on the Extremely Rapid Intensification of an Intense Tropical Cyclone: Typhoon Ida (1958). *J. Atmos. Sci.* 72, 4194–4217. doi:10.1175/jas-d-14-0247.1

Kaplan, J., and DeMaria, M. (2003). Large-scale Characteristics of Rapidly Intensifying Tropical Cyclones in the North Atlantic basin. *Wea. Forecast.* 18, 1093–1108. doi:10.1175/1520-0434(2003)018<1093:lcorit>2.0.co;2

Kaplan, J., Rozoff, C. M., DeMaria, M., Sampson, C. R., Kossin, J. P., Velden, C. S., et al. (2015). Evaluating Environmental Impacts on Tropical Cyclone Rapid Intensification Predictability Utilizing Statistical Models. *Wea. Forecast.* 30, 1374–1396. doi:10.1175/waf-d-15-0032.1

Kuang, Z., and Hartmann, D. L. (2007). Testing the Fixed Anvil Temperature Hypothesis in a Cloud-Resolving Model. *J. Clim.* 20, 2051–2057. doi:10.1175/jcli4124.1

Leighton, H., Gopalakrishnan, S., Zhang, J. A., Rogers, R. F., Zhang, Z., and Tallapragada, V. (2018). Azimuthal Distribution of Deep Convection, Environmental Factors, and Tropical Cyclone Rapid Intensification: A Perspective from HWRF Ensemble Forecasts of Hurricane Ddouard (2014). *J. Atmos. Sci.* 75, 203–227. doi:10.1175/jas-d-17-0171.1

Li, X., Davidson, N. E., Duan, Y., Tory, K. J., Sun, Z., and Cai, Q. (2020). Analysis of an Ensemble of High-Resolution WRF Simulations for the Rapid Intensification of Super Typhoon Rammasun (2014). *Adv. Atmos. Sci.* 37, 187–210. doi:10.1007/s00376-019-8274-z

Lin, Y.-L., Farley, R. D., and Orville, H. D. (1983). Bulk Parameterization of the Snow Field in a Cloud Model. *J. Clim. Appl. Meteorol.* 22, 1065–1092. doi:10.1175/1520-0450(1983)022<1065:bpotsf>2.0.co;2

Merrill, R. T. (1988). Characteristics of the Upper-Tropospheric Environmental Flow Around Hurricanes. *J. Atmos. Sci.* 45, 1665–1677. doi:10.1175/1520-0469(1988)045<1665:cotute>2.0.co;2

Mlawer, E. J., Taubman, S. J., Brown, P. D., Iacono, M. J., and Clough, S. A. (1997). Radiative Transfer for Inhomogeneous Atmospheres: RRTM, a Validated Correlated-K Model for the Longwave. *J. Geophys. Res.* 102, 16663–16682. doi:10.1029/97jd00237

Molinari, J., Dodge, P., Vollaro, D., Corbosiero, K. L., Jr., and Marks, F. (2006). Mesoscale Aspects of the Downshear Reformation of a Tropical Cyclone. *J. Atmos. Sci.* 63, 341–354. doi:10.1175/jas3591.1

Molinari, J., Vollaro, D., and Corbosiero, K. L. (2004). Tropical Cyclone Formation in a Sheared Environment: A Case Study. *J. Atmos. Sci.* 61, 2493–2509. doi:10.1175/jas3291.1

Montgomery, M., and Smith, R. (2014). Paradigms for Tropical Cyclone Intensification. *Amoj* 64, 37–66. doi:10.22499/2.6401.005

Montgomery, M. T., Nicholls, M. E., Cram, T. A., and Saunders, A. B. (2006). A Vortical Hot Tower Route to Tropical Cyclogenesis. *J. Atmos. Sci.* 63, 355–386. doi:10.1175/jas3604.1

Montgomery, M. T., Zhang, J. A., and Smith, R. K. (2014). An Analysis of the Observed Low-Level Structure of Rapidly Intensifying and Mature Hurricane Earl (2010). *Q.J.R. Meteorol. Soc.* 140, 2132–2146. doi:10.1002/qj.2283

Moon, Y., and Nolan, D. S. (2010). The Dynamic Response of the hurricane Wind Field to Spiral Rainband Heating. *J. Atmos. Sci.* 67, 1779–1805. doi:10.1175/2010jas3171.1

Nolan, D. S., Moon, Y., and Stern, D. P. (2007). Tropical Cyclone Intensification from Asymmetric Convection: Energetics and Efficiency. *J. Atmos. Sci.* 64, 3377–3405. doi:10.1175/jas3988.1

Pratt, A. S., and Evans, J. L. (2009). Potential Impacts of the Saharan Air Layer on Numerical Model Forecasts of North Atlantic Tropical Cyclogenesis. *Wea. Forecast.* 24, 420–435. doi:10.1175/2008waf2007090.1

Rhome, J. R., Sisko, C. A., and Knabb, R. D. (2006). "On the Calculation of Vertical Shear: An Operational Perspective," in 27th Conference. On Hurricanes And Tropical Meteorology, Monterey, CA, April 27, 2006. American. Meteorological. Society. Available at: https://ams.confex.com/ams/27Hurricanes/techprogram/paper_108724.htm

Riemer, M., and Laliberté, F. (2015). Secondary Circulation of Tropical Cyclones in Vertical Wind Shear: Lagrangian Diagnostic and Pathways of Environmental Interaction. *J. Atmos. Sci.* 72, 3517–3536. doi:10.1175/jas-d-14-0350.1

Riemer, M., Montgomery, M. T., and Nicholls, M. E. (2010). A New Paradigm for Intensity Modification of Tropical Cyclones: Thermodynamic Impact of Vertical Wind Shear on the Inflow Layer. *Atmos. Chem. Phys.* 10, 3163–3188. doi:10.5194/acp-10-3163-2010

Rivoire, L., Birner, T., and Knaff, J. (2016). Evolution of the Upper-Level thermal Structure in Tropical Cyclones. *Geophys. Res. Lett.* 43 (10), 530–537. doi:10.1002/2016gl070622

Rogers, R. F., Reasor, P. D., and Zhang, J. A. (2015). Multiscale Structure and Evolution of Hurricane Earl (2010) during Rapid Intensification. *Mon. Wea. Rev.* 143, 536–562. doi:10.1175/mwr-d-14-00175.1

Rogers, R. F., Zhang, J. A., Zawislak, J., Jiang, H., Alvey, G. R., Zipser, E. J., et al. (2016). Observations of the Structure and Evolution of hurricane Edouard (2014) during Intensity Change. Part II: Kinematic Structure and the Distribution of Deep Convection. *Mon. Wea. Rev.* 144, 3355–3376. doi:10.1175/mwr-d-16-0017.1

Rogers, R., Reasor, P., and Lorsolo, S. (2013). Airborne Doppler Observations of the Inner-Core Structural Differences between Intensifying and Steady-State Tropical Cyclones. *Mon. Wea. Rev.* 141, 2970–2991. doi:10.1175/mwr-d-12-00357.1

Ruppert, J. H., and Hohenegger, C. (2018). Diurnal Circulation Adjustment and Organized Deep Convection. *J. Clim.* 31, 4899–4916. doi:10.1175/jcli-d-17-0693.1

Ryglicki, D. R., Cossuth, J. H., Hodyss, D., and Doyle, J. D. (2018a). The Unexpected Rapid Intensification of Tropical Cyclones in Moderate Vertical Wind Shear. Part I: Overview and Observations. *Mon. Wea. Rev.* 146, 3773–3800. doi:10.1175/mwr-d-18-0020.1

Ryglicki, D. R., Doyle, J. D., Hodyss, D. H., Cossuth, J. H., Jin, Y., Viner, K. C., et al. (2019). The Unexpected Rapid Intensification of Tropical Cyclones in Moderate Vertical Wind Shear Part III: Outflow-Environment Interaction. *Mon. Wea. Rev.* 14 (8), 2919–2940. doi:10.1175/mwr-d-18-0370.1

Ryglicki, D. R., Doyle, J. D., Jin, Y., Hodyss, D., and Cossuth, J. H. (2018b). The Unexpected Rapid Intensification of Tropical Cyclones in Moderate Vertical Wind Shear. Part II: Vortex Tilt. *Mon. Wea. Rev.* 146, 3801–3825. doi:10.1175/mwr-d-18-0021.1

Sanger, N. T., Montgomery, M. T., Smith, R. K., and Bell, M. M. (2014). An Observational Study of Tropical Cyclone Spinup in Supertyphoon Jangmi (2008) from 24 to 27 September. *Mon. Wea. Rev.* 142, 3–28. doi:10.1175/mwr-d-12-00306.1

Shi, D. L., and Chen, G. H. (2021). Double Warm-Core Structure and Potential Vorticity Diagnosis during the Rapid Intensification of Supertyphoon Lekima (2019). *J. Atmos. Sci.* 78 (8), 2471–2492. doi:10.1175/jas-d-20-0383.1

Smith, R. K., and Montgomery, M. T. (2015). Toward Clarity on Understanding Tropical Cyclone Intensification. *J. Atmos. Sci.* 72, 3020–3031. doi:10.1175/jas-d-15-0017.1

Smith, R. K., Zhang, J. A., and Montgomery, M. T. (2017). The Dynamics of Intensification in a Hurricane Weather Research and Forecasting Simulation of Hurricane Earl (2010). *Q.J.R. Meteorol. Soc.* 143, 293–308. doi:10.1002/qj.2922

Tang, B., and Emanuel, K. (2010). Midlevel Ventilation's Constraint on Tropical Cyclone Intensity. *J. Atmos. Sci.* 67, 1817–1830. doi:10.1175/2010jas3318.1

Tang, B., and Emanuel, K. (2012). Sensitivity of Tropical Cyclone Intensity to Ventilation in an Axisymmetric Model. *J. Atmos. Sci.* 69, 2394–2413. doi:10.1175/jas-d-11-0232.1

Titley, D. W., and Elsberry, R. L. (2000). Large Intensity Changes in Tropical Cyclones: A Case Study of Supertyphoon Flo during TCM-90. *Mon. Wea. Rev.* 128, 3356–3573. doi:10.1175/1520-0493(2000)128<3556:licitc>2.0.co;2

Vigh, J. L., and Schubert, W. H. (2009). Rapid Development of the Tropical Cyclone Warm Core. *J. Atmos. Sci.* 66, 3335–3350. doi:10.1175/2009jas3092.1

Wadler, J. B., Zhang, J. A., Jaimes, B., and Shay, L. K. (2018). Downdrafts and the Evolution of Boundary Layer Thermodynamics in Hurricane Earl (2010) before and during Rapid Intensification. *Mon. Wea. Rev.* 146, 3534–3565. doi:10.1175/mwr-d-18-0090.1

Wang, B., and Xie, X. (1996). Low-Frequency Equatorial Waves in Vertically Sheared Zonal Flow. Part I: Stable Waves. *J. Atmos. Sci.* 53 (3), 449–467. doi:10.1175/1520-0469(1996)053<0449:lfewiv>2.0.co;2

Wang, B., and Zhou, X. (2008). Climate Variation and Prediction of Rapid Intensification in Tropical Cyclones in the Western North Pacific. *Meteorol. Atmos. Phys.* 99, 1–16. doi:10.1007/s00703-006-0238-z

Wang, Y., Rao, Y., Tan, Z.-M., and Schönemann, D. (2015). A Statistical Analysis of the Effects of Vertical Wind Shear on Tropical Cyclone Intensity Change over the Western North Pacific. *Mon. Wea. Rev.* 143, 3434–3453. doi:10.1175/mwr-d-15-0049.1

Wang, Y., and Wu, C.-C. (2004). Current Understanding of Tropical Cyclone Structure and Intensity Changes? a Review. *Meteorol. Atmos. Phys.* 87, 257–278. doi:10.1007/s00703-003-0055-6

Willoughby, H. E. (1998). Tropical Cyclone Eye Thermodynamics. *Mon. Wea. Rev.* 126, 3053–3067. doi:10.1175/1520-0493(1998)126<3053:tcet>2.0.co;2

Wong, M. L. M., and Chan, J. C. L. (2004). Tropical Cyclone Intensity in Vertical Wind Shear. *J. Atmos. Sci.* 61, 1859–1876. doi:10.1175/1520-0469(2004)061<1859:tciivw>2.0.co;2

Zeng, Z., Chen, L., and Wang, Y. (2008). An Observational Study of Environmental Dynamical Control of Tropical Cyclone Intensity in the Atlantic. *Mon. Wea. Rev.* 136, 3307–3322. doi:10.1175/2008mwr2388.1

Zeng, Z., Wang, Y., Duan, Y., Chen, L., and Gao, Z. (2010). On Sea Surface Roughness Parameterization and its Effect on Tropical Cyclone Structure and Intensity. *Adv. Atmos. Sci.* 27, 337–355. doi:10.1007/s00376-009-8209-1

Zeng, Z., Wang, Y., and Wu, C.-C. (2007). Environmental Dynamical Control of Tropical Cyclone Intensity-An Observational Study. *Mon. Wea. Rev.* 135, 38–59. doi:10.1175/mwr3278.1

Zhang, D.-L., and Kieu, C. Q. (2006). Potential Vorticity Diagnosis of a Simulated Hurricane. Part II: Quasi-Balanced Contributions to Forced Secondary Circulations. *J. Atmos. Sci.* 63, 2898–2914. doi:10.1175/jas3790.1

Zhang, F., and Tao, D. (2013). Effects of Vertical Wind Shear on the Predictability of Tropical Cyclones. *J. Atmos. Sci.* 70, 975–983. doi:10.1175/jas-d-12-0133.1

Zhang, X., Duan, Y., Wang, Y., Wei, N., and Hu, H. (2017). A High-Resolution Simulation of Supertyphoon Rammasun (2014)-Part I: Model Verification and Surface Energetics Analysis. *Adv. Atmos. Sci.* 34, 757–770. doi:10.1007/s00376-017-6255-7

Conflict of Interest: The authors declare that the research was conducted in the absence of any commercial or financial relationships that could be construed as a potential conflict of interest.